Kinetics for Zinc Ion Induced *Sepia Pharaonis* Arginine Kinase Inactivation and Aggregation

Yue-Xiu Si[1,2,¶], Jinhyuk Lee[3,4,¶], Juan-Ge Cheng[2], Shang-Jun Yin[2], Yong-Doo Park[2,5], Guo-Ying Qian[2,*], and Xia-Min Jiang[1,*]

[1]School of Marine Sciences, Ningbo University, Ningbo 315211, P.R. China; [2]College of Biological and Environmental Sciences, Zhejiang Wanli University, Ningbo 315100, P.R China; [3]Korean Bioinformation Center, Korea Research Institute of Bioscience and Biotechnology, Daejeon 305-806, Korea; [4]Department of Nanobiotechnology and Bioinformatics, Korea University of Science and Technology, Daejeon 305-350, Korea; [5]Zhejiang Provincial Key Laboratory of Applied Enzymology, Yangtze Delta Region Institute of Tsinghua University, Jiaxing 314006, P.R. China

Xia-Min Jiang

Abstract: Arginine kinase is an essential enzyme which is closely related to energy metabolism in marine invertebrates. Arginine kinase provides a significant role in quick response to environmental change and stress. In this study, we simulated a tertiary structure of *Sepia pharaonis* arginine kinase (SPAK) based on the gene sequence and conducted the molecular dynamics simulations between SPAK and Zn^{2+}. Using these results, the Zn^{2+} binding sites were predicted and the initial effect of Zn^{2+} on the SPAK structure was elucidated. Subsequently, the experimental kinetic results were compared with the simulation results. Zn^{2+} markedly inhibited the activity of SPAK in a manner of non-competitive inhibitions for both arginine and ATP. We also found that Zn^{2+} binding to SPAK resulted in tertiary conformational change accompanying with the hydrophobic residues exposure. These changes caused SPAK aggregation directly. We screened two protectants, glycine and proline, which effectively prevented SPAK aggregation and recovered the structure and activity. Overall, our study suggested the inhibitory effect of Zn^{2+} on SPAK and Zn^{2+} can trigger SPAK aggregation after exposing large extent of hydrophobic surface. The protective effects of glycine and proline against Zn^{2+} on SPAK folding were also demonstrated.

Keywords: Aggregation, arginine kinase, Zn^{2+}, inhibition, molecular dynamics simulation, *Sepia pharaonis*.

1. INTRODUCTION

The cuttlefish *Sepia pharaonis* belongs to cephalopods, and it is an important marine resource for human consumption [1]. *Sepia pharaonis* has excellent breeding prospects based on its characteristics of larger body type, fast growth and suitability for high-density cultivation. At present, research into the artificial breeding of *Sepia pharaonis* is being carried out in China. It has shown that *Sepia pharaonis* is particularly sensitive to environmental changes in its breeding environment [2]. Changes in salinity and heavy metal concentration cause a severe stress reaction, including stress-induced inking behavior, and can even lead to massive death. Thus, it is important to study the stress response of cephalopods and their defense mechanisms under different environmental conditions.

Previous studies have indicated that energy metabolism-related enzymes in invertebrates are importantly responsible for adapting the environmental stress. In this regard, arginine

kinase (AK, EC 2.7.3.3) is distinctively found in marine invertebrates to be associated with adapting the environmental troubles caused from physical and chemical factors [3-6]. AK is a phosphagen kinase that catalyzes the reversible reaction of phosphoryl group's transfer from various sources of phosphagens [7, 8]. It has been generally recognized that AK plays a pivotal role in ATP buffering in invertebrates both temporal and extreme conditions where muscle and nerves cells require immediate and high fluctuating energy demands via catalyzing Mg^{2+} cofactor dependent phosphoryl transfer [9, 10]. The evolution of a marine organism's metabolic patterns generally involves further adaptation to the aquatic environment and this was supported by the homologous sequence alignments of various origins of AKs [11-13]. Some of divalent metal ions (i.e. Cd^{2+}, Cu^{2+} and Pb^{2+}) were found to have significant inhibitory effects on AK catalysis, which could directly affect the body's energy balance and destroy energy homeostasis in invertebrates [5, 14-15].

Cuttlefish muscle is a good food source of some important essential minerals [16-18]. However, the increasing pollution of seawater by metal ions often leads to excessive intracellular unfavorable accumulation. Excessive Zn^{2+} can be toxic to marine organisms regardless of that Zn^{2+} is a basic ingredient of several important enzymes and displays multiple functions in the catalytic reaction [19-20]. It is evident that Zn^{2+} binding directly mediates hydrophobic exposure of

*Addresses correspondence to these authors at the School of Marine Sciences, Ningbo University, Ningbo 315211, P.R. China, Tel: 86-57487600171; Fax: 86-57487608347; E-mail: jiangxiamin@nbu.edu.cn; and at the College of Biological and Environmental Sciences, Zhejiang Wanli University, Ningbo 315100, P.R China; Tel: 86-57488222298; Fax: 86-57488222298; E-mail: qianguoying_wanli@hotmail.com

¶These authors equally contributed to this study.

enzyme active site pocket and structural unfolding, as well as unfavorable aggregation in a broad variety of metallic/non-metallic enzymes, including creatine kinase and AK [21,22]. The roles of Zn^{2+} in ocean invertebrates have not been well elucidated, but it has been found that Zn^{2+} concentrations in the body of marine organisms, especially for marine inverte-brates, are more excessive than other organisms' metabo-lisms [23-25]. The reason of Zn^{2+} can exist excess concentra-tion in tissues of marine invertebrates is that it is prone to bind to macromolecules or present as insoluble metal inclu-sions in tissues [26]. It has rarely been reported the role of Zn^{2+} on enzymes' structure and function in aquatic organ-isms and thus, it could be a topic of interest to investigate the role of excess Zn^{2+} on enzyme derived from aquatic organ-ism such as *Sepia pharaonis* that is one of food source for human. Accordingly, we elucidated the inhibitory effect of Zn^{2+} on arginine kinase from *Sepia pharaonis* (SPAK) in this study and the protective functional role of some osmolytes against Zn^{2+} in controlling changes in enzyme structure and function and combined these studies with ORF gene se-quence analysis and computational simulations. Exploration the basic characteristics of the energy metabolism related enzymes might provide significant message on the metabolic adaptation mechanisms during environmental stress.

2. MATERIALS AND METHODS

2.1. Materials

Magnesium acetate, thymol blue, ATP, arginine, ANS, zinc acetate dehydrate were obtained from Sigma-Aldrich (Shanghai, China). Sephacryl S-200 and Cellulose DE-52 were purchased from GE Healthcare (Piscataway, NJ, USA) and Whatman (GE Healthcare), respectively. The other chemicals were the analytical grade and locally obtained.

2.2. cDNA Cloning of SPAK and RACE

Total RNA was extracted from tissue samples of healthy adult *S. Pharaonis* using a Trizol RNA extraction reagent (Invitrogen, Carlsbad, USA). Oligo (dT) primer was used to initiate the reverse transcription process, and cDNA synthe-sis was conducted by M-MLV reverse transcriptase (Takara, Shiga, Japan). Partial fragments of the AK gene from the prepared cDNA were obtained with primers AK-F and AK-R (Table **1**). The purified PCR products were subcloned into pMD18-T vector (Takara). Positive clones were sequenced.

The missing cDNA sequences of the SPAK gene were then obtained by 3'-RACE and 5'-RACE using RACE Kit in accordance with the manufacturer's instructions (Takara). For 3' RACE, RT product was amplified with nested for-ward PCR primers (3' RACE1 and 3' RACE2) to obtain the partial sequence and an adaptor primer. PCR was performed under hot-start conditions (95ºC, 3 min) for 33 cycles of 94ºC 30 s, 58ºC 30 s, and 72ºC 60 s, and then 7 min at 72ºC. The oligo-dC primer and terminal deoxynucleotidyl trans-ferase was used to amplify the 5'-half of the SPAK cDNA. Outer PCR was carried out by 5'RACE1 and 5'RACE Outer Primer. Inner PCR was conducted by 5'RACE2 and 5'RACE Inner Primer. PCR amplification was performed for 33 cycles of 94ºC 30 s, 68ºC 30 s, and 72ºC 60 s, and then 7

Table 1. The Primers Used for RACE and cDNA Cloning of SPCK.

Primer	Sequence (5'—3')
AK-F	TTGCTGAAGTCCTTGATGCYGT
AK-R	TCATGGTRGTACCCAAGTTGC
3'RACE1	TGGCAGAGGAATTTACTTCAACCAGGACA
3'RACE2	GAAGAAATTGACCTTTGCCAAGAAGGA-TAACA
5'RACE1	CAGTCAGCTTCTGTTGAGTGTCTGGGGT
5'RACE2	GCCTGCAGAGCTTCAACTGAGACCTTC
5'RACE Outer Primer	GCCACGCGTCGACTAGTACGGGGGGGGGG
5'RACE Inner Primer	GGCCACGCGTCGACTAGTAC

min at 72ºC. Finally, the amplified products were subcloned and sequenced, respectively. The sequences were spliced and analyzed using BLAST in the GenBank database.

2.3. Computational Simulations of SPAK

The pseudo quadratic restraint with simulated annealing method (PQR-SA) [27] was used to establish a SPAK ho-mology model. A knowledge-based statistical energy poten-tial (STAP) was used [28] for higher protein like scores. All simulations and analyses were used in the CHARMM pro-gram. To validate the structure model, the radius of gyration of the protein and the associated protein-like scores were measured. A functional study of the structure, dockable pocket site prediction (DPSP) was used and identified the appropriate ligand-binding pocket. To understand the role of Zn^{2+} in SPAK, molecular dynamics simulations (MD) were prepared with the action of Zn^{2+}. The experimental concen-tration was calculated, and eight Zn^{2+} ions were randomly added in the simulation. Ten-nanosecond (ns) MD simula-tions were carried out and the atomic coordinates were saved every 1 picosecond (ps) for further analyses. The protein stabilities were checked by root mean square deviation of the alpha carbon relative to its initiating structure. The bound Zn^{2+} ions were counted as a function of time. Protein flexi-bilities were checked based on the feature of residue number by root mean square fluctuation (RMSF). The final structures after 10 ns MD simulations were applied to determine the secondary structure and to compare the two structures with and without Zn^{2+}. The secondary structure ratio was tested by DSSP [29].

2.4. SPAK Purification and Activity Assay

SPAK enzyme samples were extracted and purified from the muscle of cuttlefish by homogenate, cellulose DE-52 ion-exchange chromatography and Sephacryl S-200 gel chroma-tography according the previous procedures [30,31]. AK activity was determined by monitoring H^+ generation in the catalytic reaction of ATP and arginine with an indicator

thymol blue as the previous reported methods [31,32]. The absorption change value per minute was measured at 575 nm by a Shimadzu UV-1800 spectrophotometer. The OD value at 280 nm was measured to calculate the protein content using the corresponding standard curve based on bull serum albumin.

2.6. Kinetic Analysis

The Lineweaver-Burk equation of non-competitive inhibition in double-reciprocal form is as follows, and it was used to analysis the inhibition type and kinetics:

$$\frac{1}{v} = \frac{K_m}{V_{max}}(1 + \frac{[I]}{K_i})\frac{1}{[S]} + \frac{1}{V_{max}}(1 + \frac{[I]}{K_i}) \qquad (1)$$

The secondary replot can be established from the following equation:

$$Y\text{-}intercept = \frac{1}{V_{max}} + \frac{1}{K_i V_{max}}[I] \qquad (2)$$

The values including V_{max}, K_m and K_i, can be calculated from the two equations and the corresponding figures. When the obtained data in the secondary replot shown in Eq. (2) is linearly well fitted, it assumes that the inhibitor binding site is a single class.

2.7. Protein Unfolding Measurement Induced by Zn^{2+}

For the protein unfolding measurement, various concentrations of Zn^{2+} was incubated with SPAK for 2 h at 20 °C.
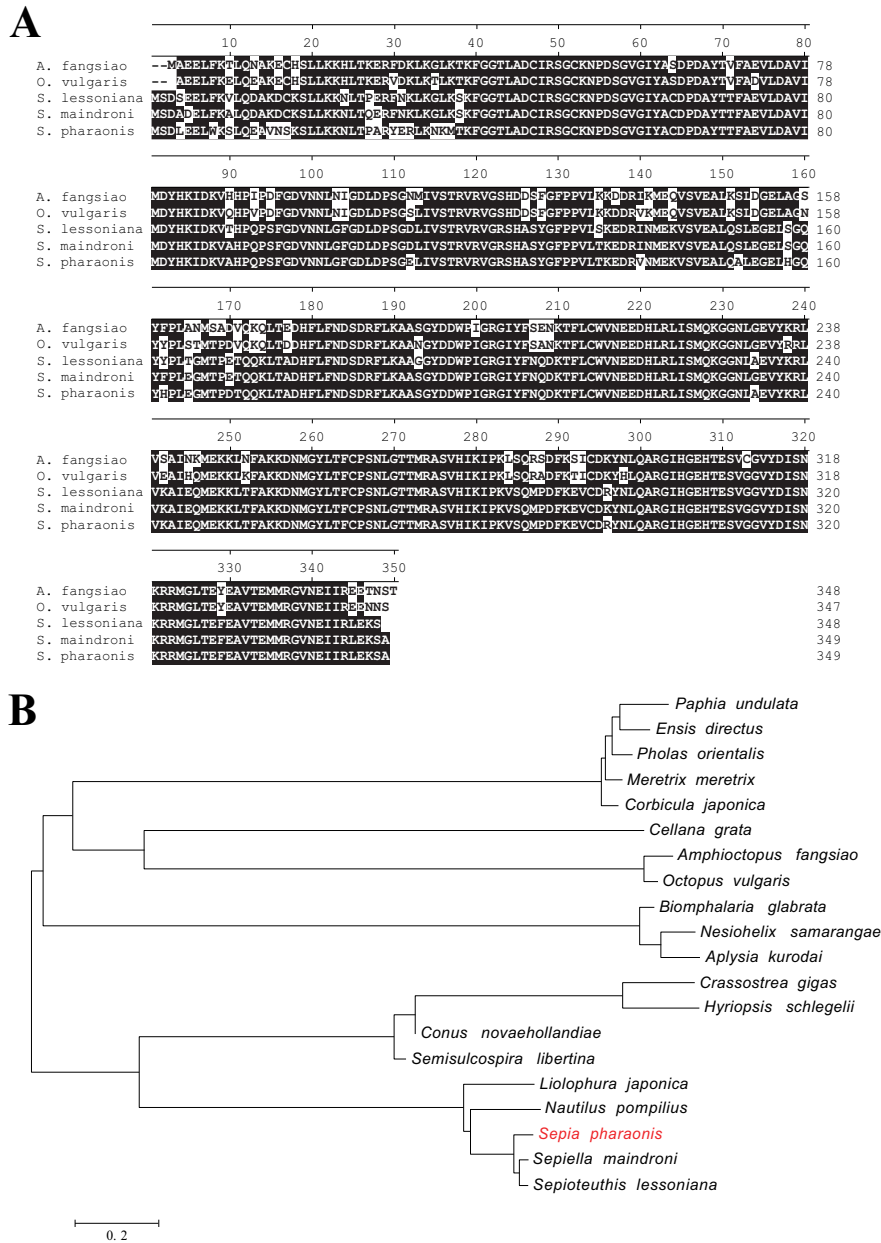
Figure 1. Multiple alignment and neighbor-joining tree of SPAK. (**A**) Multiple sequence alignments of SPAK with five other homologous arginine kinase amino acid sequences. (**B**) Phylogenetic relationship of the AK amino acid sequences. MEGA4 software was used to construct the neighbor-joining tree.

Fluorescence emission spectra were measured using a F-4500 spectrofluorometer (Hitachi, Japan) according the previous procedures [33]. Intrinsic fluorescence was measured following excitation at 280 nm. The emission wavelength was from 300 to 400 nm. Zn^{2+}-treated SPAK was incubated with 40 μM ANS for 30 min in the dark to probe the hydrophobic surface. The excitation and emission wavelengths for ANS-binding fluorescence of SPAK were 380 nm and 420-600 nm, respectively. The Zn^{2+} mediated aggregation of SPAK was followed by the absorbance record at 400 nm. All above measurements were performed in the buffer (20 mM Tris-acetic acid, pH 8.0).

RESULTS

3.1. RACE and Gene Cloning of SPAK

The SPAK gene sequences were successfully amplified and submitted to GenBank under the accession number 1799738. The SPAK cDNA comprises 1251 bp with an 1050 bp open reading frame. The BLAST results displayed more than 80% similarity to AKs of *Sepiella maindroni* (AEK26855.1), *Sepioteuthis lessoniana* (BAA95610.1), *Octopus vulgaris* (BAA95609.1) and *Amphioctopus fangsiao* (AEK65120.1) (Fig. **1a**). Phylogenetic analysis result displayed that SPAK sequences closely clustered with the homologous AKs from mollusca followed by cuttlefish, octopus, chiton, oyster, conch and clam (Fig. **1b**).

3.2. Homology Modeling and Molecular Dynamics Simulations of SPAK

A SPAK structure model was created using the homology modeling method (Fig. **2a**). The template structures used were 1m15, 1qh4, 3jpz, 3l2f, 2k9i, 2ba3, 1p94, and 2cpg (PDB entry codes). The best template was 1m15 with a sequence identity of 55%. The radius of gyration of SPAK was lower than the standard value of the same size of SPAK (green dot in Fig. **2b**). This indicates that the model was more tightly packed than the X-ray structures. The protein like scores were measured and marked on the high resolution X-ray structure space (Fig. **2c**). The clash and Ramachandran related scores (WhatRama, MolRama, ProRama, and rotamer) had good indicators comparable to the X-ray experimental structures. From these results, the developed homology model was shown to be a useful protein model for further study, such as docking and simulations.

The DPSP server was used to predict plausible ligands for SPAK. DPSP identified an ADP binding site with high DPSP score (Fig. **3**). The interacting residues are shown in Figure **3a** as yellow spheres (residue numbers: 118 120 176 179 181 215 218 223 227 274 278 302 304 305 306 307 317).

After 10 ns simulations, protein flexibility and Zn bound ligand residues were sought (Fig. **4a**). The Zn interacting residues are highlighted in red at the bottom of Fig. 4a. The ADP binding sites are shown marked with blue at the bottom of Fig. 4a. Two Zn^{2+} overlapped in the ADP binding sites, while the other five Zn^{2+} didn't overlap (Fig. **4b**). Thus the Zn^{2+} can interfere with SPAK, and may cause inactivity of
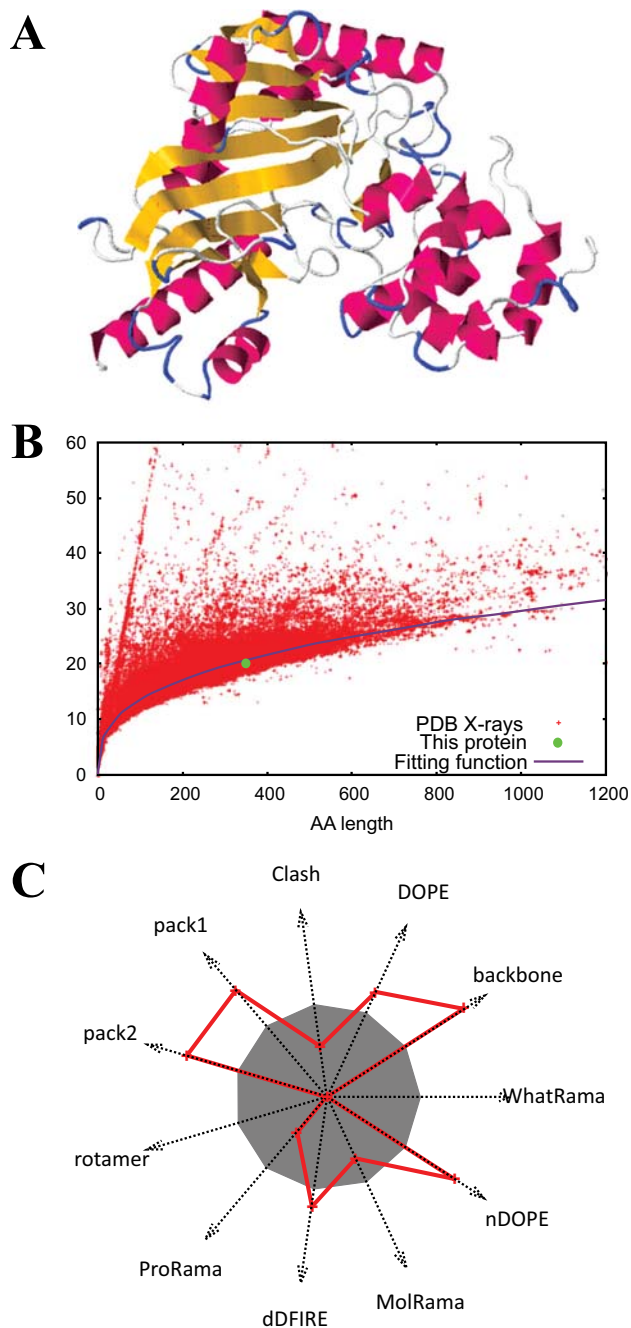
Figure 2. Homology protein model of SPAK. (**A**) The developed homology model of SPAK. The protein structure is drawn as a cartoon image colored red (α helix) and yellow (β sheet). (**B**) The radius of gyration (Rg) is indicated by total residue number. The SPAK structure is indicated by the green dot. The best fitting curve for X-ray structures is shown in blue. (**C**) The protein like scores of the SPAK homology model structure in X-ray structure space. The shaded grey circle represents the high 50% X-ray structure scores.

SPAK at a high concentration of Zn^{2+}. The final two structures were superimposed (Fig. **4c**) and the secondary structures were aligned according to the residues (Fig. **4d**). The backbone similarity of the two structures is 3.2 Å. The
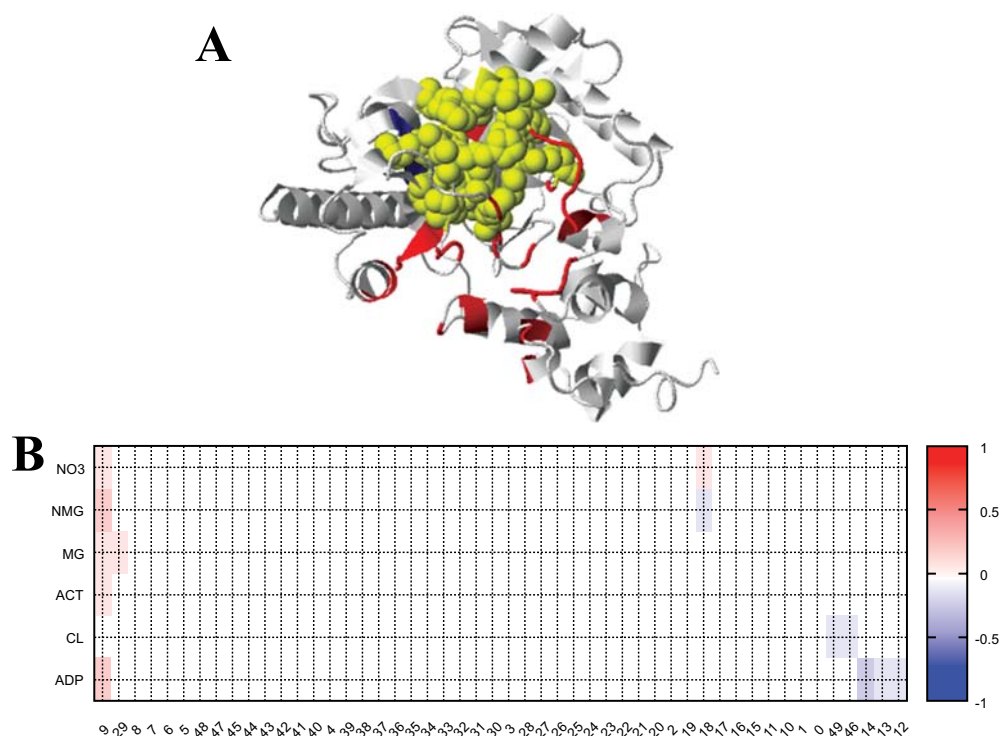
Figure 3. Predicted ADP binding site of SPAK. (**A**) SPAK protein structure with plausible ADP binding sites (shown as yellow spheres in the structure view and yellow circles in the heat map figure). (**B**) The heat map of DPSP scores. The darker red color indicates a higher affinity binding site. The X- and Y-axes represent pocket numbers and found ligand lists. (The color version of the figure is available in the electronic copy of the article).
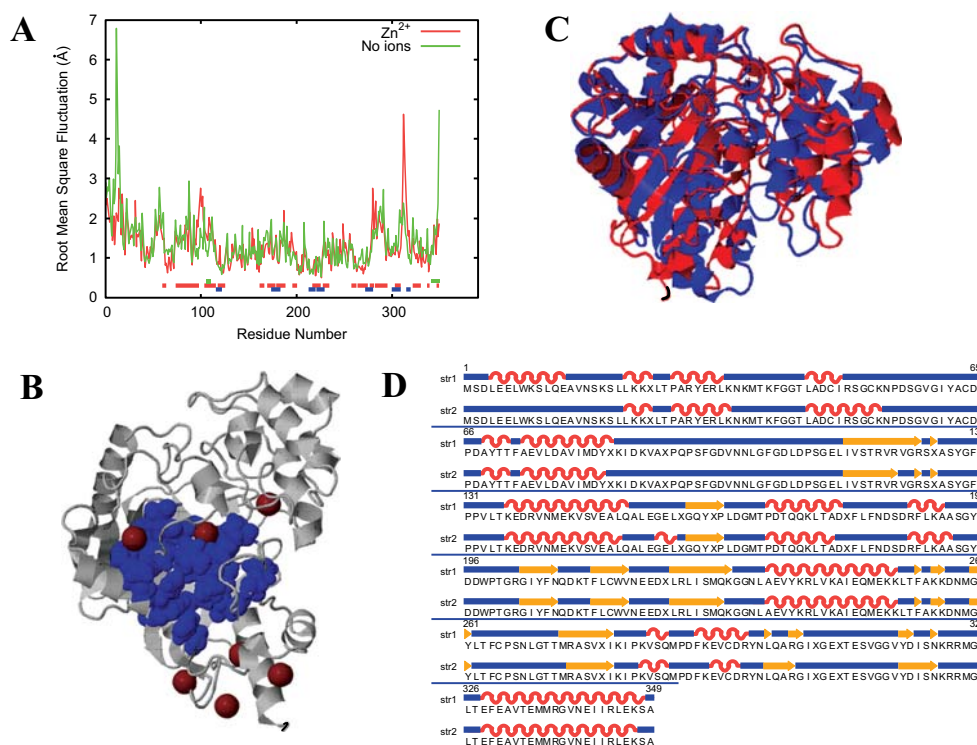

Figure 4. Structural analyses of SPAK with Zn^{2+}. (**A**) RMSF plot with (red line)/without (green line) Zn^{2+}. The Zn^{2+} bound sites are marked by squares in the bottom plot (red: final structure, green: initial structure, and blue: plausible ADP binding site predicted by DPSP). (**B**) The final structure with Zn^{2+}. ADP binding sites and Zn^{2+} are indicated by blue and brown spheres, respectively. (**C**) The final structures with (red) and without (blue) bound Zn^{2+}. (**D**) The secondary structure schemes showing the differences between the final structures. Str1/str2 represent with/without Zn^{2+}, respectively. The α-helix, β-sheet and coil are indicated by red, yellow and blue patterns, respectively. (The color version of the figure is available in the electronic copy of the article).

secondary structure ratios of the two structures are very similar, and no great structural change was found although the first simulation was in the presence of Zn^{2+}. In subsequent kinetic studies, we attempted to validate the simulation results with respect to activity modulation and conformational changes due to Zn^{2+} binding.

3.3. SPAK Activity Inhibition by Zn^{2+}

SPAK was mixed with different concentrations of Zn^{2+} for 2 h at 20 °C and measured the relative activity. The results showed that Zn^{2+} inhibited AK activity with a concentration related pattern (Fig. **5**). Relative SPAK activity remained about 15% when the Zn^{2+} concentration was greater than 0.03 mM (Fig. **5a**). Measurement of the IC_{50} gave a value of 10.6 ± 0.6 μM ($n = 3$). SPAK could be refolded due to the dilution effect in the Zn^{2+} absent substrate system (Fig. **5b**). The relative SPAK activity remained about 25% when the Zn^{2+} concentration was greater than 0.03 mM. The IC_{50} value was 11.2 ± 0.8 μM ($n = 3$).
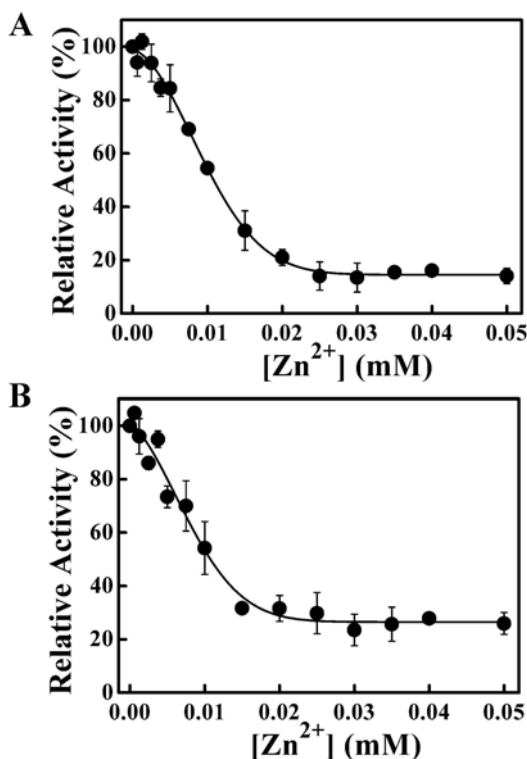
Figure 5. The activity inhibition of Zn^{2+} on SPAK. Different concentrations of Zn^{2+} was incubated with SPAK for 2 h in buffer (20 mM Tris-acetic acid, pH 8.0) at 20°C, followed the relative activity measurement with corresponding Zn^{2+} concentrations (**A**) or without Zn^{2+} (**B**). The final concentration of SPAK was 0.06 μM. Data are presented as average values, *n=3*.

3.4. Noncompetitive Inhibition Induced by Zn^{2+}

Double-reciprocal Lineweaver–Burk plots were used to determine the inhibition type and mechanisms of Zn^{2+}. The results showed changes in the values of apparent V_{max}. The inhibition induced by Zn^{2+} was non-competitive mode for arginine (Fig. **6a**) and ATP (Fig. **6c**). The secondary plot (*Y-intercept* versus [Zn^{2+}]) was linear (Fig. **6b** and Fig. **6d**), indicating that the SPAK inhibition site of Zn^{2+} was single or

single class. The K_i values were 11.17 ± 0.87 mM for arginine and 5.31 ± 0.61 mM for ATP. The dynamic constants of SPAK were $K_m = 0.36 \pm 0.08$ mM and $V_{max} = 57.81 \pm 6.72$ U/mg for arginine and $K_m = 5.11 \pm 0.75$ mM and $V_{max} = 46.78 \pm 4.96$ U/mg for ATP. The result of noncompetitive inhibition indicated that Zn^{2+} could bind SPAK, and that Zn^{2+} might reduce the enzyme activity by impacting its tertiary structure. To verify our supposition, the tertiary structure changes of SPAK incuced by Zn^{2+} were measured.

3.5. Zn^{2+}-Induced Tertiary Structural Change and Aggregation of SPAK

The intrinsic and ANS-binding fluorescence measurements were conducted to determine the tertiary structural changes of SPAK treated with different concentrations of Zn^{2+}. Addition of Zn^{2+} at different concentrations resulted in a slight red-shift from 329 to 332 nm according to the maximum emission peak wavelength of intrinsic fluorescence (Fig. **7a**). The intensity changed from about 190 A.U. to 240 A.U., while the concentration of Zn^{2+} changed from 0 to 0.15 mM, and then declined to about 200 A.U. (Fig. **7b**). This finding indicated that the binding of Zn^{2+} did loosen the structure of SPAK and slightly induced the tertiary structural change. The ANS-binding fluorescence spectra measurements showed that Zn^{2+} significantly enhanced the ANS-binding fluorescence of the enzyme with the increase of concentration. The resulted indicated that the combination of enzyme with Zn^{2+} induced hydrophobic surface exposure (Figs. **7c** and **7d**). The hydrophobic disruption of SPAK could directly lead to protein misfolding and aggregation with the loss of enzymatic activity. Next, Zn^{2+}-mediated SPAK aggregation was tested and the results showed that SPAK aggregation increased remarkably as the Zn^{2+} concentration increased (Fig. **8**).

### 3.6. Screening for Protective Osmolytes on the Inactivation of SPAK

Osmolytes can act as folding chaperones and protect the enzyme activity by facilitating the correct folding of protein. We screened the protective agents for Zn^{2+} mediated inactivation from five common osmolytes (glycine, proline, glycerol, liquaemin and sucrose). The experiment results showed that glycine and proline were efficient protective agents for SPAK activity among these osmolytes. SPAK was mixed with 0.03 mM Zn^{2+} (an effective SPAK-inactivated concentration) and the different concentrations of osmolytes, respectively. The activity of SPAK was significantly restored by glycine and proline in a concentration dependent manner (Figs. **9a** and **9b**). At a glycine concentration of 50 mM, 86% of the activity was restored. Surprisingly, approximately 100% of the enzyme activity was restored after incubation with 120 mM proline. However, glycerol, sucrose and liquaemin showed no protective function for SPAK activity in Zn^{2+} mediated inactivation (Figs. **9c** to **9e**).

3.7. Effect of Glycine and Proline on the SPAK Tertiary Structure and Aggregation

The structure protective effect of glycine and proline was tested through the ANS-binding fluorescence of 0.02 mM Zn^{2+}-treated SPAK. The two osmolytes both obviously
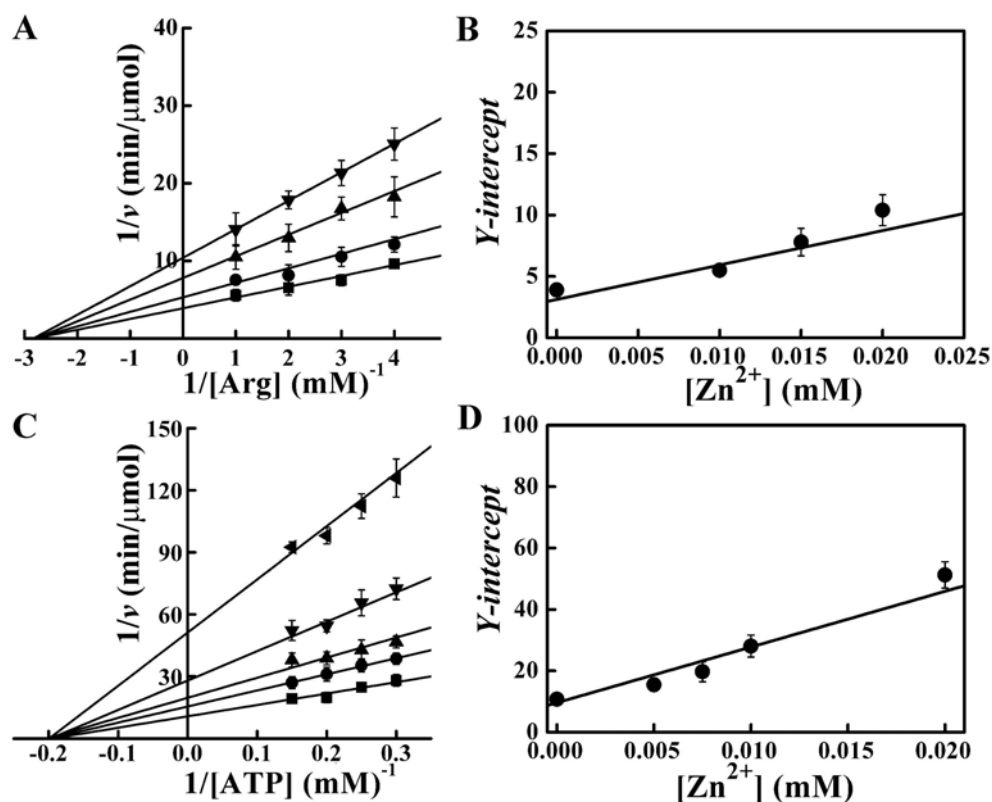
Figure 6. Double-reciprocal plot in the presence of Zn^{2+}. (A) Lineweaver-Burk plot for arginine. Zn^{2+} concentrations were 0 (■), 0.01 (●), 0.015 (▲) and 0.02 (▼) mM, respectively. The concentration of ATP was 5 mM, and the final concentration of the enzyme was 0.12 μM. (B) The secondary plot for arginine. Data was derived from (A). (C) Lineweaver-Burk plot for ATP. Zn^{2+} concentrations were 0 (■), 0.005 (●), 0.075 (▲), 0.01 (▼) and 0.02 (◄) mM, respectively. The concentration of arginine was 5.7 mM, and the final concentration of the enzyme was 0.06 μM. (D) The secondary plot for ATP. Data was derived from (C).
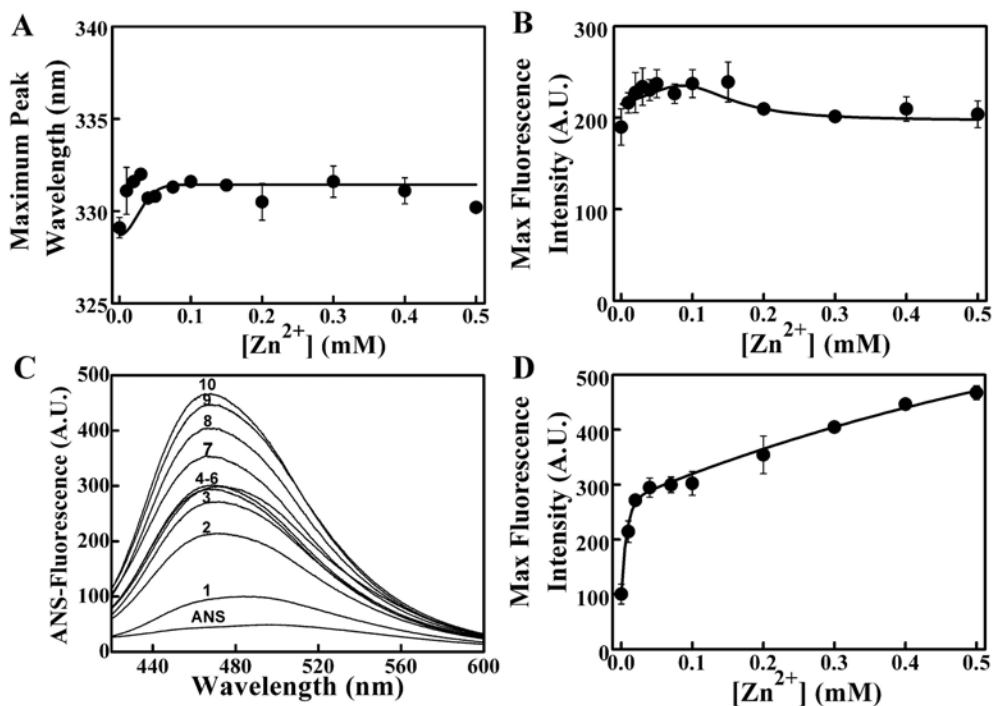
Figure 7. Fluorescence changes of SPAK induced by Zn^{2+}. (A) Maximum peak wavelength of intrinsic fluorescence versus $[Zn^{2+}]$. (B) Maximum intrinsic fluorescence intensity versus $[Zn^{2+}]$. (C) ANS-binding fluorescence changes of SPAK. The labels 1 to 10 indicate 0, 0.01, 0.02, 0.04, 0.07, 0.1, 0.2, 0.3, 0.4 and 0.5 mM Zn^{2+}. (D) Maximum ANS-fluorescence intensity changes. Data was derived from (C). The final concentration of SPAK was 5 μM.
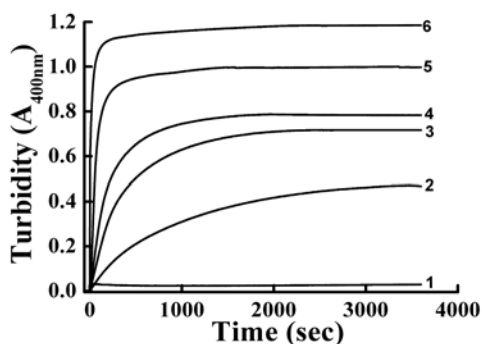
Figure 8. SPAK aggregation induced by Zn^{2+}. Labeled 1-6 represented 0, 0.05, 0.1, 0.2, 0.3 and 0.5 mM Zn^{2+}, respectively. The final concentration of SPAK was 17 μM and the measurement was carried out at 20 °C.
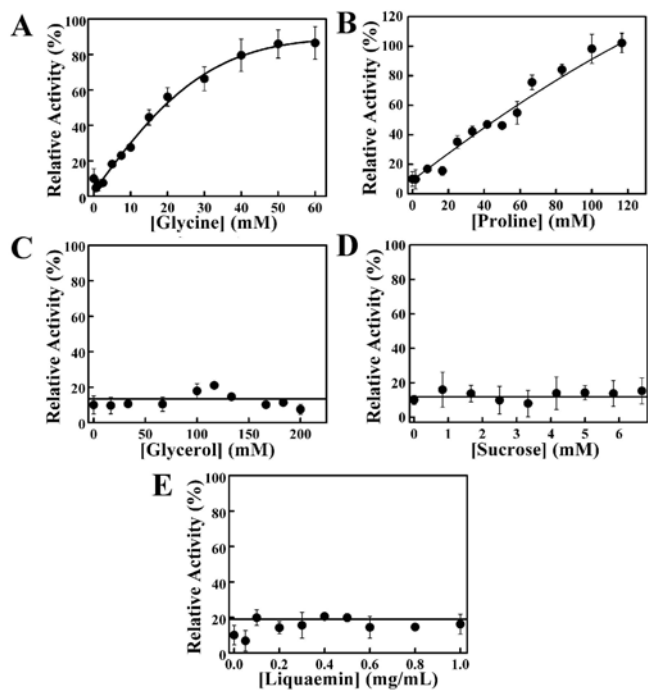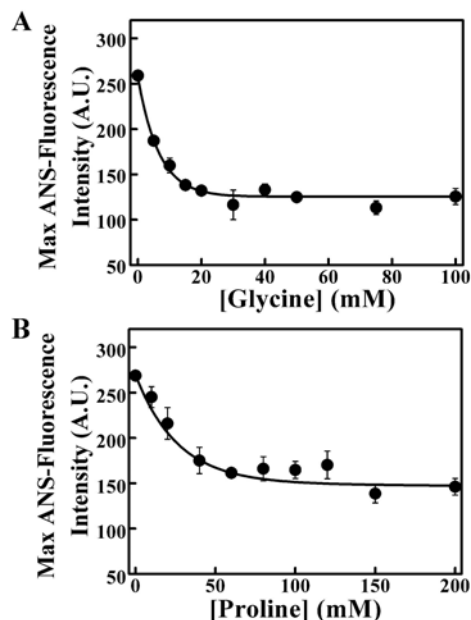

Figure 9. Osmolytes screening for SPAK reactivation. Different concentrations of glycine (A), proline (B), glycerol (C), sucrose (D) and liquaemin (E) were incubated with SPAK (inactivated by 0.03 mM Zn^{2+}) for 2 h at 20 °C, respectively. The relative activity was tested, and the final concentration of SPAK was 0.06 μM.

Figure 10. Prevention of Zn^{2+}-induced SPAK hydrophobic surface changes. The effects of glycine (A) and proline (B) were assayed by the ANS-fluorescence of SPAK (treated with 0.02 mM Zn^{2+}). The enzyme concentration was 5 μM.

Figure 11. Prevention of Zn^{2+}-induced SPAK aggregation. (A) The protective effect of glycine. Labeled 1 to 5 represented 0, 1, 2, 4 and 5 mM glycine, respectively. (B) The protective effect of proline. Labeled 1 to 6 represented 0, 50, 60, 70, 80 and 100 mM proline, respectively. The concentrations of SPAK and Zn^{2+} were 17 μM and 0.5 mM, respectively.
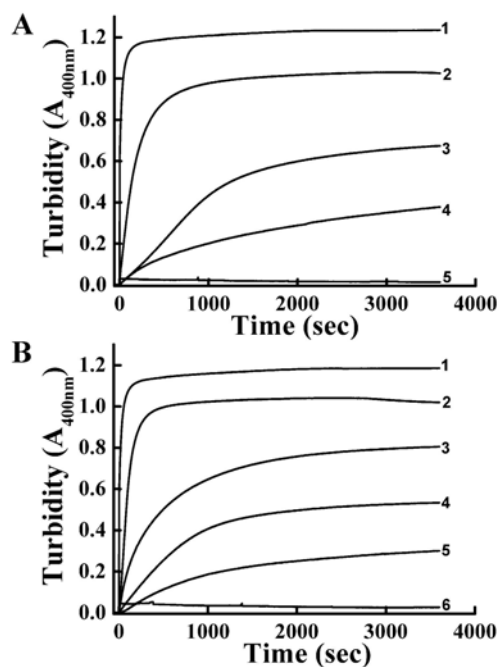
reduced the Zn^{2+}-induced surface hydrophobicity with the increase of concentrations (Fig. **10**). It showed that the recover of SPAK activity could depend mainly on the restoration of the structure. Zn^{2+} induced aggregation of SPAK was effectively reduced by glycine or proline (Fig. **11**). Either 5 mM glycine or 100 mM proline could thoroughly prevent SPAK aggregation. Glycine and proline could act as folding chaperones by the structural protection and aggregation prevention of SPAK.

4. DISCUSSION

The SPAK gene sequence obtained using the RACE technique was first revealed in this study. On the basis of the gene sequence results, we obtained a reasonable 3D structure of SPAK and carried out molecular dynamics simulation for SPAK with the binding of Zn^{2+}. The overall predicted results implied that Zn^{2+} was a tight binding ligand and could directly affect the catalytic function of SPAK. The subsequent

kinetic experiments confirmed that Zn^{2+} inhibited SPAK with a non-competitive inhibition mode. Zn^{2+} generated significant hydrophobic surface exposure and tertiary structure change of SPAK along with aggregation occurrence. The exposure of the hydrophobic groups caused by Zn^{2+} binding could directly result in misfolding of SPAK and thus modulated enzyme activity.

We found that among the osmolytes tested, glycine and proline not only prevented aggregation but also restored the activity and tertiary structure of SPAK that were destroyed due to the unfolding induced by Zn^{2+}. These results implied that glycine and proline may regulate the activity and function of arginine kinase on unsuitable environmental conditions. The function of osmolytes in heavy metal poisoning preventment could be an interesting topic for marine invertebrates' research.

Since the applied concentration of Zn^{2+} in this study was comparable to physiological *Sepia pharaonis* body condition, our results could be useful to elucidate the function of excessive Zn^{2+} in SPAK as a negative effecter. To illuminate more detail physiological functions of Zn^{2+} and of the osmolytes *in vivo* for SPAK and the relationship during SPAK unfolding, including the Zn^{2+}-mediated SPAK aggregation problem, more systematic subsequent and sequential experiments should be conducted in the further studies.

5. CONCLUSION

We revealed the inhibitory effects of Zn^{2+} on SPAK by using computational MD simulation integrating enzymatic kinetics. Our results suggest concrete *in vitro* evidence of the toxicity and negative regulation of Zn^{2+} for arginine kinase in *Sepia pharaonis* and also suggest a putative protective role of osmolytes against Zn^{2+}. The methodological approach for investigate target enzyme integrating with simulations could be applicable for the other enzymes from various ocean invertebrates. This study elucidates the mechanisms underlying Zn^{2+}-related functions in cephalopods, and will help further clarify the stress mechanisms of cuttlefish under inhospitable environmental conditions.

LIST OF ABBREVIATIONS

SPAK   =   arginine kinase from *Sepia pharaonis*

ANS   =   1-anilinonaphthalene-8-sulfonate

ATP   =   adenosine triphosphate

MD   =   molecular dynamics

CONFLICT OF INTEREST

The authors confirm that this article content has no conflict of interest.

ACKNOWLEDGEMENTS

REFERENCES

[1]   Sikorski, Z.E.; Kolodziejska, I. The composition and properties of squid meat. *Food. Chem.*, **1986**, *20*, 213-224.

[2]   Le, K.X.; Jiang, X.M.; Peng, R.B.; Luo, J.; Tang, F.; Wang, C.L. Effects of four ecological factors on the growth and survival of *Sepia pharaonis* larvae. *J. Biol.*, **2014**, *31*, 33-37.

[3]   Kinsey, S.T.; Lee, B.C. The effects of rapid salinity change on in vivo arginine kinase flux in the juvenile blue crab, *Callinectes sapidus*. *Comp. Biochem. Physiol. B*, **2003**, *135*, 521-531.

[4]   Abe, H.; Hirai, S.; Okada, S. Metabolic responses and arginine kinase expression under hypoxic stress of the kuruma prawn *Marsupenaeus japonicus*. *Comp. Biochem. Physiol. A*, **2007**, *146*, 40-46.

[5]   Silvestre, F.; Dierick, J.F.; Dumont, V.; Dieu, M.; Raes, M.; Devos, P. Differential protein expression profiles in anterior gills of *Eriocheir sinensis* during accl imation to cadmium. *Aquat. Toxicol.*, **2006**, *76*, 46-58.

[6]   Morris, S.; van Aardt, W.J.; Ahern, M.D. The effect of lead on the metabolic and energetic status of the Yabby, Cherax destructor, during environment al hypoxia. *Aquat. Toxicol.*, **2005**, *75*, 16-31.

[7]   Ellington, W.R. Evolution and physiological roles of phosphagen systems. *Annu. Rev. Physiol.*, **2001**, *63*, 289-325.

[8]   Buttlaire, D.H.; Cohn, M. Interaction of manganous ion, substrates, and anions with arginine kinase. Magnetic relaxation rate studies of water protons and kinetic anion effects. *J. Biol. Chem.*, **1974**, *249*, 5733-5740.

[9]   Shofer, S.L.; Willis, J.A.; Tjeerdema, R.S. Effects of hypoxia and toxicant exposure on arginine kinase function as measures by ^{31}P-NMR magnetization transfer in living abalone. *Comp. Biochem. Physiol. C*, **1997**, *117*, 283-289.

[10]   Voncken, F.; Gao, F.; Wadforth, C.; Harley, M.; Colasante, C. The phosphoarginine energy-buffering system of trypanosoma brucei involves multiple arginine kinase isoforms with different subcellular locations. *Plos One*, **2013**, *8*, e65908.

[11]   Suzuki, T.; Furukohri, T. Evolution of phosphagen kinase. Primary structure of glycocyamine kinase and arginine kinase from invertebrates. *J. Mol. Biol.*, **1994**, *237*, 353-357.

[12]   Furukohri, T.; Okamoto, S.; Suzuki, T. Evolution of phosphagen kinase (III). Amino acid sequence of arginine kinase from the shrimp *Penaeus japonicus*. *Zool. Sci.*, **1994**, *11*, 229-234.

[13]   Azzi, A.; Clark, S.A.; Ellington, W.R.; Chapman, M.S. The role of phosphagen specificity loops in arginine kinase. *Protein Sci.*, **2004**, *13*, 575-585.

[14]   Silvestre, F.; Dierick, J.F.; Dumont, V.; Dieu, M.; Raes, M.; Devos, P. Differential protein expression profiles in anterior gills of *Eriocheir sinensis* during acclimation to cadmium. *Aquat. Toxicol.*, **2006**, *76*, 46-58.

[15]   Zhou, Q.; Wu, C.G.; Dong, B.; Li, F.H.; Liu, F.Q.; Xiang, J.H. Proteomic analysis of acute responses to copper sulfate stress in larvae of the brine shrimp, *Artemia sinica*. *Chin. J. Oceanol. Limn.*, **2010**, *28*, 224-232.

[16]   Ichihashi, H.; Kohno, H.; Kannan, K.; Tsumura, A.; Yamasaki, S. Multielement analysis of purpleback flying squid using high resolution inductively coupled plasma-mass spectrometry (HR ICP-MS). *Environ. Sci. Technol.*, **2001**, *35*, 3103-3108.

[17]   Bustamante, P.; Grigiono, S.; Boucher-Rodoni, R.; Caurant, F.; Miramand, P. Bioaccumulation of 12 trace elements in the tissues of the *Nautilus Nautilus* mae-romphalus from New Caledonia. *Mar. Pollut. Bull.*, **2000**, *40*, 688-696.

[18] Craing, S.; Overnell, J. Metal in squid, *Loligo forbesi*, adults, eggs and hatchings. No evidence for a role for Cu- or Zn-methallothionein. *Comp. Biochem. Physiol. C*, **2003**, *134*, 311-317.

[19] Jacobsen, J.A.; Major Jourden, J.L.; Miller, M.T.; Cohen, S.M. To bind zinc or not to bind zinc: an examination of innovative approaches to improved metalloproteinase inhibition. *Biochim. Biophys. Acta*, **2010**, *1803*, 72-94.

[20] Fukada, T.; Yamasaki, S.; Nishida, K.; Murakami, M.; Hirano, T. Zinc homeostasis and signaling in health and diseases: Zinc signaling. *J. Biol. Inorg. Chem.*, **2011**, *16*, 1123-1134.

[21] Tong, X.; Zeng, X.; Zhou, H.M. Effects of zinc on creatine kinase: activity changes, conformational changes, and aggregation. *J. Protein Chem.*, **2000**, *19*, 553-562.

[22] Liu, T.; Wang, X. Zinc induces unfolding and aggregation of dimeric arginine kinase by trapping reversible unfolding intermediate. *Acta Biochim. Biophys. Sin.*, **2010**, *42*, 779-786.

[23] Shyn, A.; Chalk, S.J.; Smith, K.; Charnock, N.L.; Bielmyer, G.K. Zinc distribution in the organs of adult *Fundulus heteroclitus* after waterborne zinc exposure in freshwater and saltwater. *Arch. Environ. Contam. Toxicol.*, **2012**, *63*, 544-553.

[24] Núñez-Nogueira, G.; Fernández-Bringas, L.; Ordiano-Flores, A.; Gómez-Ponce, A.; de León-Hill, C.P.; González-Farías, F. Accumulation and regulation effects from the metal mixture of Zn, Pb, and Cd in the tropical shrimp *Penaeus vannamei*. *Biol. Trace Elem. Res.*, **2012**, *150*, 208-213.

[25] Mitra, A.; Chowdhury, R.; Banerjee, K. Concentrations of some heavy metals in commercially important finfish and shellfish of the River Ganga. *Environ. Monit. Assess*, **2012**, *184*, 2219-2230.

[26] Eisler, R. Zinc Hazards to Fish, Wildlife, and Invertebrates: A Synoptic Review. *Contaminant Hazard Reviews Report*, **1993**, *26*, 1-126.

[27] Kim, T.R.; Oh, S.; Yang, J.S.; Lee, S.; Shin, S.; Lee, J. A simplified homology-model builder toward highly protein-like structures: an inspection of restraining potentials. *J. Comput. Chem.*, **2012**, *33*, 1927-1935.

[28] Kim, T.R.; Yang, J.S.; Shin, S.; Lee, J. Statistical torsion angle potential (STAP) energy functions for protein structure modeling: a bicubic interpolation approach. *Proteins*, **2013**, *81*, 1156-1165.

[29] Kabsch, W.; Sander, C. Dictionary of protein secondary structure: pattern recognition of hydrogen-bonded and geometrical features. *Biopolymers*, **1983**, *22*, 2577-2637.

[30] Si, Y.X.; Lee, J.; Yin, S.J.; Gu, X.X.; Park, Y.D.; Qian, G.Y. The inhibitory effects of Cu^{2+} on *Exopalaemon carinicauda* arginine kinase via inhibition kinetics and molecular dynamics simulations. *Appl. Biochem. Biotechnol.*, **2015**, *176*, 1217-1236.

[31] Si, Y.X.; Lee, J.; Zhao, F.; Yin, S.J.; Park, Y.D.; Qian, G.Y.; Jiang, X.M. Effects of cadmium on the cuttlefish *Sepia pharaonis*' arginine kinase: unfolding kinetics integrated with computational simulations. *J. Biomol. Struct. Dyn.*, **2015**, *19*, 1-15.

[32] Yu, Z.; Pan, J.; Zhou, H.M. A direct continuous pH-spectrophotometric assay for arginine kinase activity. *Protein Pept. Lett.*, **2002**, *9*, 545-552.

[33] Yin, S.J.; Si, Y.X.; Chen, Y.F.; Qian, G.Y.; Lu, Z.R.; Oh, S.; Lee, J.; Lee, S.; Yang, J.M.; Lee D.Y.; Park, Y.D. Mixed-Type Inhibition of Tyrosinase from *Agaricus bisporus* by Terephthalic Acid: Computational Simulations and Kinetics. *Protein J.*, **2011**, *30*, 273-280.